

pubs.acs.org/NanoLett Letter

Tuning the Properties of Zero-Field Room Temperature Ferromagnetic Skyrmions by Interlayer Exchange Coupling

Roberto Lo Conte,* Ashis K. Nandy,* Gong Chen, Andre L. Fernandes Cauduro, Ajanta Maity, Colin Ophus, Zhijie Chen, Alpha T. N'Diaye, Kai Liu, Andreas K. Schmid,* and Roland Wiesendanger*



Cite This: Nano Lett. 2020, 20, 4739-4747



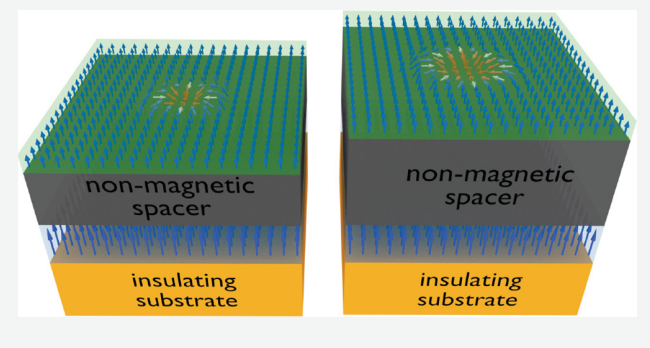
ACCESS

III Metrics & More

Article Recommendations

Supporting Information

ABSTRACT: Magnetic materials offer an opportunity to overcome the scalability and energy consumption limits affecting the semiconductor industry. New computational device architectures, such as low-power solid state magnetic logic and memory-in-logic devices, have been proposed which rely on the unique properties of magnetic materials. Magnetic skyrmions, topologically protected quasi-particles, are at the core of many of the newly proposed spintronic devices. Many different materials systems have been shown hosting ferromagnetic skyrmions at room temperature. However, a magnetic field is a key ingredient to stabilize skyrmions, and this is not desirable for applications, due to the poor scalability of active components generating magnetic fields.



Here we report the observation of ferromagnetic skyrmions at room temperature and zero magnetic field, stabilized through interlayer exchange coupling (IEC) between a *reference magnet* and a *free magnet*. Most importantly, by tuning the strength of the IEC, we are able to tune the skyrmion size and areal density. Our findings are relevant to the development of skyrmion-based spintronic devices suitable for general-use applications which go beyond modern nanoelectronics.

KEYWORDS: ferromagnetic skyrmions, non-collinear magnetism, interlayer exchange coupling, nanomagnetism, spintronics

he stabilization of magnetic skyrmions¹⁻⁴ in thin films with perpendicular magnetic anisotropy (PMA) results from the competition among different energy terms. Depending on the balance between the Heisenberg exchange interaction, the antisymmetric exchange called the Dzyaloshinskii-Moriya interaction (DMI), 5-9 and the magnetic anisotropy, a particular magnetic multilayer can have a ferromagnetic or a spin spiral ground state. When the DMI is sufficiently strong, helical-called Bloch-type-spin textures are suppressed in favor of cycloidal-called Néel-type-spin textures. In both of those ground states, the cycloidal spin textures are limited to one specific sense of rotation (lefthanded or right-handed)^{8,10} determined by the DMI sign. In the specific case of a ferromagnetic ground state, which is relevant for this work, magnetic domains are separated by Néel-type domain walls (DWs) with a unique rotational sense, as shown in Figure 1a. Finally, if a magnetic field is applied along the anisotropy axis of such a system, isolated magnetic skyrmions can be nucleated⁴ (Figure 1b).

Thin-film-based multilayers are particularly attractive for the design of potential skyrmionic devices, 11-14 due to the high tunability of their magnetic properties through materials and structural engineering. So far, room-temperature ferromagnetic skyrmions have been observed in many different multilayers. In order to make those material systems employ-

able for spintronic applications, ^{12,14,22} skyrmions must be stable without any external magnetic field. As a consequence, in the past few years, different approaches to stabilize zero-field skyrmions have been developed. ^{23–28} Those approaches are based on lateral confinement, ^{23,24} current-pulse-induced morphological thermal transitions, ²⁶ exchange bias, ²⁷ and interlayer exchange coupling. ^{25,29} The latter two approaches seem to be more suitable for practical applications, since they allow lateral transport of skyrmions and do not rely on complicated post-growth initialization processes. Furthermore, the interlayer exchange coupling is preferable to the exchange bias approach due to the tunability of the coupling and thus of the stabilized skyrmions. However, a systematic approach to fine-tune the properties of magnetic skyrmions in the absence of external magnetic fields is still missing.

Here, we report the fine-tuning of the size and areal density of ferromagnetic skyrmions at room temperature in epitaxial metallic multilayers, in the absence of external magnetic fields.

Received: January 11, 2020 Revised: May 2, 2020 Published: May 27, 2020





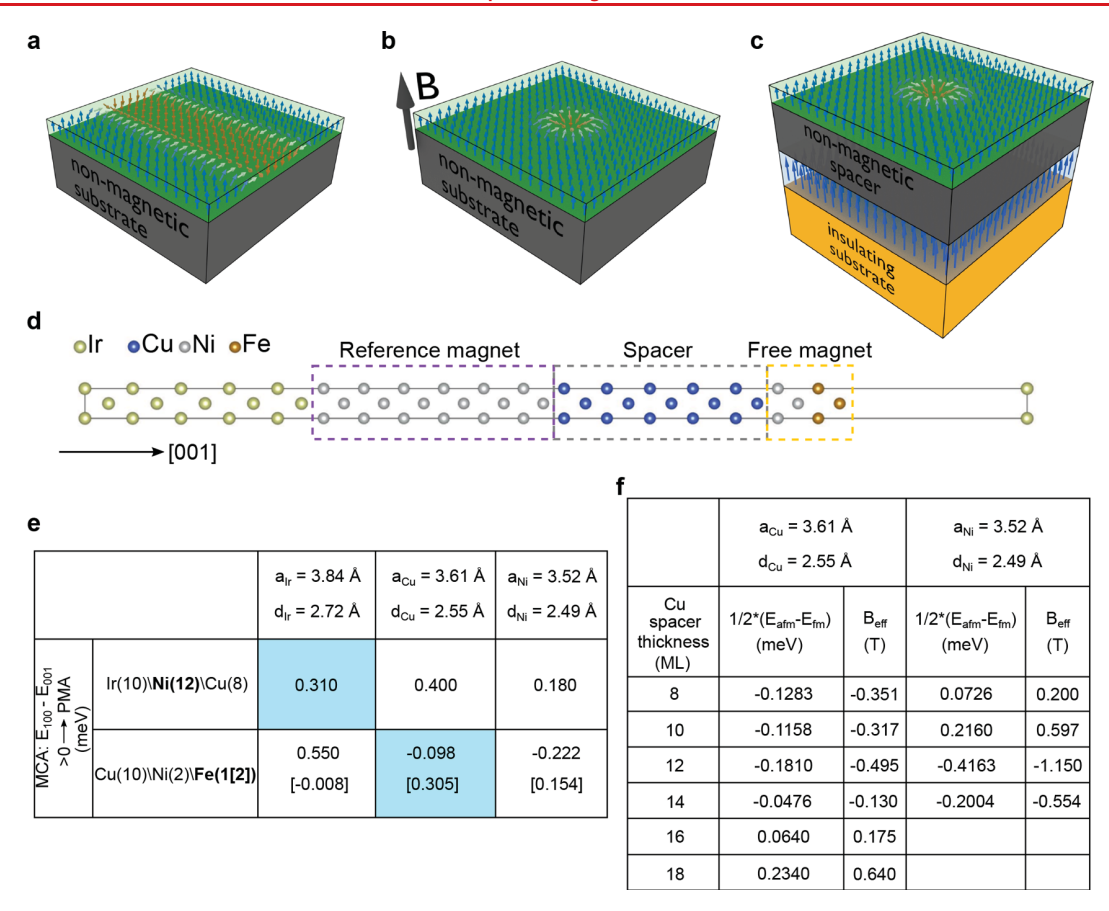


Figure 1. Interlayer exchange coupling stabilization of ferromagnetic skyrmions. (a) Schematic of a magnetic thin film hosting chiral domain walls due to interfacial DMI. (b) Stabilization of magnetic skyrmions via an external magnetic field. (c) Stabilization of magnetic skyrmions via IEC. (d) Schematic of the multilayer stack investigated by density functional theory calculations. (e) Calculated magneto-crystalline anisotropy energies for the reference and the free magnet. Three different calculations are carried out assuming an in-place lattice spacing (d_i) for the stack equal to that of Ir, Cu, and Ni, respectively. Light blue boxes indicate the values corresponding to the calculation parameters expected to be the closest to the experimental scenario. (f) Calculated IEC and corresponding effective magnetic field acting on the free magnet $(B_{\rm eff})$ as a function of the Cu spacer thickness, for two cases with in-plane lattice spacing equal to that of bulk Cu and Ni, respectively.

The epitaxial multilayers are grown on top of insulating MgO single crystals, which makes them suitable for application in spintronic devices. The mechanism used for the stabilization of the skyrmions is interlayer exchange coupling. 25,29-32 By connecting two magnetic layers through a nonmagnetic spacer, the indirect exchange coupling between the two magnetic layers is exploited in order to stabilize skyrmions at room temperature. A schematic of the multilayers investigated here is shown in Figure 1c. At the bottom of the stack, there is a thick ferromagnetic reference layer in a single domain state having all of its magnetic moments pointing in the same direction. At the top of the stack, there is a thinner magnetic free layer which, therefore, is subject to an effective magnetic field due to the magnetization of the reference layer. By changing the thickness of the nonmagnetic spacer in between the two magnets, we are able to tune the strength of the effective magnetic field, which allows us to tailor the properties of the skyrmions in the free layer.

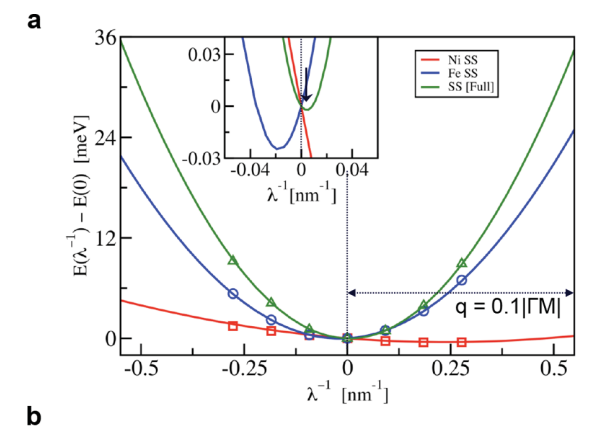
Using density functional theory (DFT) calculations as implemented in the VASP package, 33,34 we study the magnetic properties of the material stack $Ir(10)\Ni(12)\Cu(t_{Cu})\Ni(2)\Fe(1-2)$, where the thicknesses are expressed in monolayers (ML). The material system is assumed to be in a face centered cubic (fcc) structure, with the stacking along

the [001] crystallographic direction, as schematically shown in Figure 1d. The materials stack is simulated for three different conditions, where the in-plane lattice constant (bulk lattice constant) is assumed to be equal to $d_{Ir} = 2.72 \text{ Å} (a_{Ir} = 3.84 \text{ Å}),$ $d_{\text{Cu}} = 2.55 \text{ Å } (a_{\text{Cu}} = 3.61 \text{ Å}), \text{ and } d_{\text{Ni}} = 2.49 \text{ Å } (a_{\text{Ni}} = 3.52 \text{ Å})$ for Ir, Cu, and Ni, respectively. More details concerning the DFT calculations are reported in section S1 of the Supporting Information. The table in Figure 1e shows the calculated magneto-crystalline anisotropy (MCA) for the two magnetic layers. The bottom magnet $Ir(10)\backslash Ni(12)\backslash Cu(8)$ is predicted to have PMA, regardless of the chosen in-plane lattice constant (and Cu thickness, data not shown here). On the other hand, the $Cu(10)\Ni(2)\Fe(1-2)$ magnet is found to have a MCA which depends on the chosen in-plane lattice constant and the thickness of the Fe layer. As reported in the light blue box (results for calculation parameters expected to be most closely related to experimental conditions), the free magnet is predicted to have an in-plane MCA for $t_{Fe} = 1$ ML and an out-of-plane MCA for $t_{Fe} = 2$ ML. Furthermore, Figure 1f shows the calculated IEC and corresponding effective magnetic field (B_{eff}) as a function of the Cu spacer thickness. The calculations show that an interlayer exchange coupling is expected to be present in the system, with a strength that can be tuned by tailoring the thickness of the spacer. Interestingly,

calculations for stacks with different in-plane lattice spacing show different results. Therefore, we expect the actual in-plane lattice constant in the prepared stacks to play a very important role, especially in determining the sign of the IEC, ferromagnetic (>0) or anti-ferromagnetic (<0).

In order to understand the stability mechanism of magnetic DWs with a unidirectional sense of the spin rotation in the $Ni(2)\Fe(2)$ free layer, we perform total energy calculations of flat homogeneous spin spirals (SSs) characterized by SS vector \mathbf{q} along the ΓM high symmetry line in the irreducible twodimensional Brillouin zone. Our first-principle calculations are based on the full-potential linearized augmented plane wave (FLAPW) method in the film geometry as implemented in FLEUR code³⁵ (see section S1 of the Supporting Information for more details). The effective spin model describing the free magnetic layer is comprised of the exchange interaction, DMI, and MCA. The exchange and DMI constants both are the effective nearest neighbor interactions, where the former one is obtained by fitting the dispersion curve $E(\mathbf{q})$ of SSs in the vicinity of the ferromagnetic (FM) state (q = 0) without spinorbit coupling (SOC) while the latter is the result of relativistic effects within our SOC calculations. In the magnetic multilayer $\text{Cu}(001)\backslash \text{Ni}(2)\backslash \text{Fe}(2)$, it is convenient to define intralayer exchange coupling, J^{FF} and J^{NN} , for the Fe(2) layer and the Ni(2) layer on the Cu(001) substrate, respectively, and an interlayer coupling, J^{FN}, at the Ni\Fe interface. The results of our calculations for the exchange interaction and DMI constants (see section S1 of the Supporting Information for more details) are summarized in Figure 2. The SS calculations without SOC show a ferromagnetic ground state for both the magnetic layers and the full $Cu(001)\Ni(2)\Fe(2)$ system. The effective intralayer exchange constant within the Fe(2) layer, $J^{FF} = 31.1$ meV, is much stronger than that in the Ni(2) layer, $J^{NN} = 3.2$ meV, and the effective exchange constant for the full system is found to be $J_{\rm eff}$ = 46.2 meV. However, with inclusion of SOC, the systems show non-collinear ground states with opposite rotational sense, left-handed for the Fe(2) layer and right-handed for the Ni(2) layer. The DMI in Ni(2), $D^{\text{NN}} = 1.2 \text{ meV}$, is stronger than that in the Fe(2) layer, $D^{\text{FF}} =$ -0.88 meV. Because of the $C_{4\nu}$ symmetry of the film geometry, the DMI vectors around an atom are perpendicular to the bond connecting its nearest-neighbor atoms. Therefore, only Néel-type modulation of magnetizations (cycloidal SS) are supported. Figure 2a shows the dispersion curve for each magnetic layer and the full system. The energy minima show that the SS state in the Ni(2) layer is robust and the SS period is small compared to that in the Fe(2) layer. Interestingly, the ferromagnetic interlayer exchange coupling, J^{FN} = 13.5 meV, along with the layer resolved DMI constants, D^{FF} and D^{NN} , support the prediction of a magnetic state in the full system which has a right-handed rotational sense; see the inset of Figure 2a. Indeed, all of these energy contributions effectively stabilize a cycloidal SS ground state in the free layer, with a rotation period of λ = 205 nm. The effective DMI for the full system calculated within DFT is $D_{\text{eff}} = 0.32 \text{ meV} (0.16 \text{ meV}/$ atom), in good agreement with the previously reported experimental estimation, 0.12-0.17 meV/atom, by G. Chen et al.³⁶ for the materials system Cu(001)\Ni\Fe.

Next, we experimentally investigate the materials stack described above by *in situ* imaging in a spin-polarized low energy electron microscope (SPLEEM). The *in situ* capabilities of the SPLEEM allow us to observe the evolution of the magnetic state of the layer during growth as a function of its



Cu(001)\Ni(2)\Fe(2)	Fe(2) Intralayer (J ^{FF} , D ^{FF})	Ni(2) intralayer (J ^{NN} , D ^{NN})	Ni(2)\Fe(2) Interlayer (J ^{FN})	Ni(2)\Fe(2) intralayer (J _{eff} , D _{eff})
J _{nn} (meV)	31.1	3.2	13.5	46.2
D _{nn} (meV)	-0.88	1.20		0.32

Figure 2. Dzyaloshinskii-Moriya interaction calculations. (a) Energy dispersion $E(\mathbf{q})$ of the spin-spiral (SS) as a function of λ^{-1} $(q/2\pi$ in nm⁻¹) along high symmetry line \(\Gamma M. \) The continuous lines correspond to the total energy from the model with effective exchange constant and DMI which are obtained by fitting the SS energy without SOC and layer resolved SOC contributions, respectively. The symbols are the calculated energy points close to the Γ -point. Red, blue, and green refer to Ni(2), Fe(2), and $Ni(2)\Fe(2)$, respectively. The black arrow in the inset denotes the lowest energy state of the full system. (b) Effective nearest neighbor exchange constants, $J_{\rm nn}$ ($J^{\rm FF}$, $J^{\rm NN}$, $J^{\rm FN}$, $J_{\rm eff}$), and DMI, $D_{\rm nn}$ ($D^{\rm FF}$, $D^{\rm NN}$, $D_{\rm eff}$), obtained from fitting the energy dispersion of SSs calculated within DFT without and with SOC, respectively. The intralayer exchange constants are calculated assuming effectively a one-atom model for the Fe(2), Ni(2), and full $Cu(001)\backslash Ni(2)\backslash Fe(2)$ layers. The effective values for the full stack are reported in the last column on the right.

thickness. The out-of-plane (OOP)-magnetized reference magnet made of 12 ML of Ni is deposited on an Ir(001)-(1 \times 1) buffer layer grown on top of an insulating MgO(001) single crystal substrate (see the schematic in Figure 3a). Once the Ni layer is deposited, we saturate its magnetization state with an external magnetic field of $\mu_0 H = -0.5$ T, resulting in a single domain state with magnetic moments pointing down. Afterward, we deposit the Cu spacer and finally the top magnet, which consists of 2 ML of Ni and \sim 2.0–2.5 ML of Fe.

We begin our experimental investigation by exploring the interlayer coupling in this materials system. This is done by imaging the OOP magnetic state of the Ni(2)\Fe(2.5) free layer as a function of the thickness of a wedge-shaped Cu spacer, $t_{\rm Cu}$ (details about the growth of the wedged Cu spacer are available in section S9 of the Supporting Information). It is worth noting that, in agreement with the DFT calculations, a PMA is obtained only for $t_{\rm Fe} > 1$ ML, allowing us to observe OOP domains for $t_{\rm Fe} = 1.5-2.5$ ML (no OOP contrast is observed for $t_{\rm Fe} \le 1$ ML). The investigation of the wedged sample reveals the presence of a ferromagnetic coupling between the two magnets over the entire range of the Cuwedge thickness (0–35 ML), with a strength that varies as a function of $t_{\rm Cu}$. This is shown in Figure 3b, where we report the normalized difference between the fractional areas of

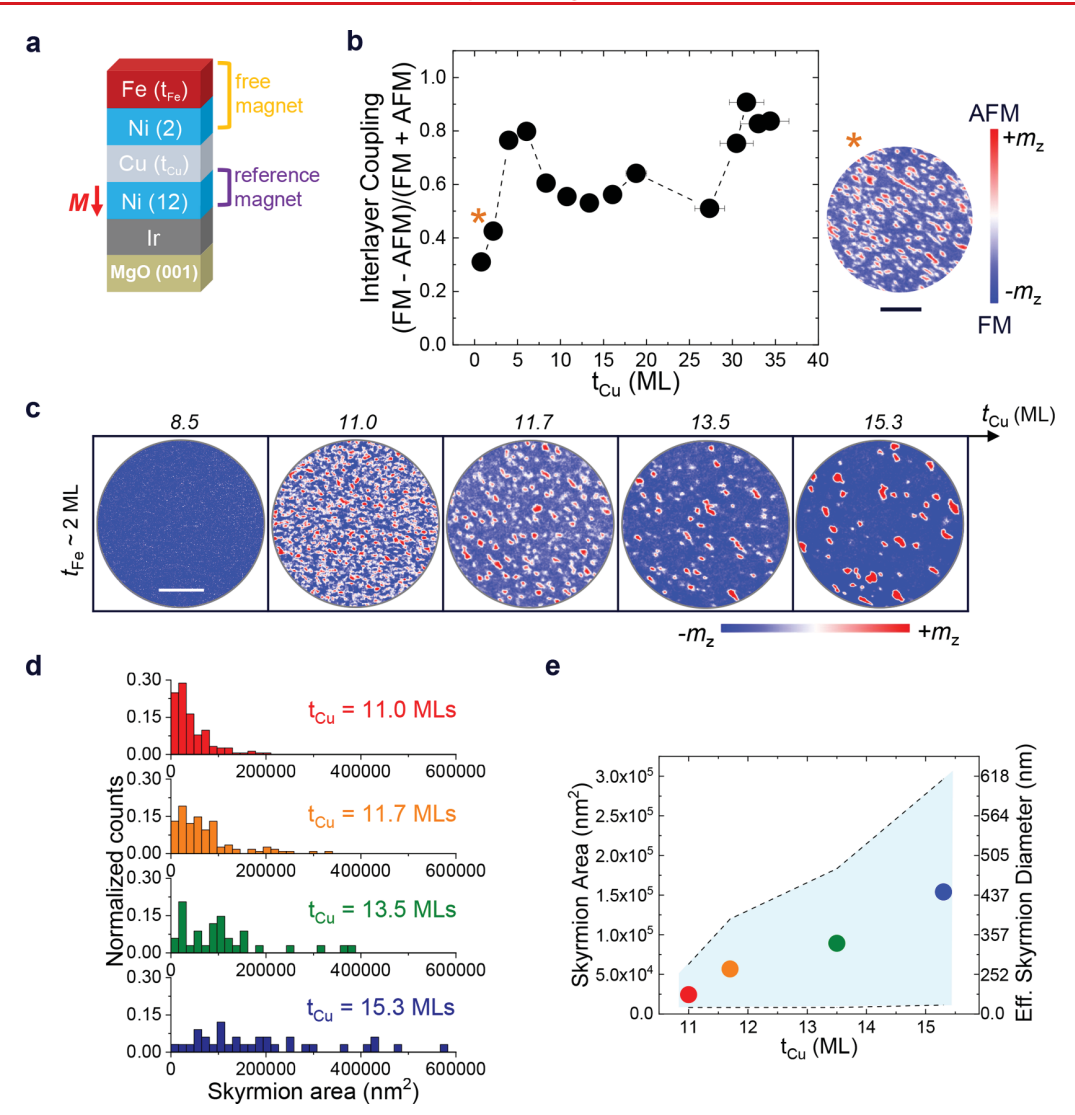


Figure 3. Tuning the properties of zero-field ferromagnetic skyrmions via IEC. (a) Schematic of the [001]-oriented multilayer stack investigated in this work, made of a magnetic Ni(12) reference layer and a Ni(2)\Fe(2-2.5) free layer. The numbers in parentheses indicate the thickness in monolayers [ML]. The reference layer is prepared with its magnetic state pointing down (see small red arrow). (b) The essence of the interlayer coupling, determined from the normalized difference between the areas covered by domains aligned ferromagnetically (FM) and antiferromagnetically (AFM) with respect to the reference magnet, as a function of t_{Cu} for a sample having a wedged Cu spacer and $t_{\text{Fe}} = 2.5$ ML. One of the images used for such analysis is shown on the right. The scale bar is 2 μ m. (c) Evolution of the OOP magnetic state in the free layer of a series of samples with different t_{Cu} . The scale bar is 2 μ m. (d) Distribution of the magnetic skyrmion area for the samples with $t_{\text{Cu}} = 11.0$, 11.7, 13.5, and 15.3 ML. (e) Median values of skyrmion area and effective skyrmion diameters extracted from the histograms in panel d. The blue shaded area represents the standard deviation of the skyrmion area distributions in panel d.

ferromagnetically (FM) and anti-ferromagnetically (AFM) coupled domains, (FM - AFM)/(FM + AFM) observed in a 10 μm field-of-view, as a function of $t_{\rm Cu}$. This ratio gives us information about the sign (>0, ferromagnetic; <0, anti-ferromagnetic) and the varying strength of the interlayer coupling between free and reference magnets. As visible in the graph in Figure 3b, even though the sign of the IEC is the same for all of the investigated $t_{\rm Cu}$ values, its amplitude is modulated by $t_{\rm Cu}$, revealing an oscillatory-like behavior. This points to a Ruderman–Kittel–Kasuya–Yosida (RKKY) type of coupling, $^{30-32,37,38}$ where its amplitude is expected to oscillate as a function of the spacer's thickness, even though no change in the sign of the IEC is observed. This is a very surprising and interesting result, and more details about the nature of the magnetic coupling in our samples can be found in section S8 of

the Supporting Information. Indeed, when compared with the calculated IEC values reported in Figure 1f, the experimentally observed coupling does not follow the predicted sign change. Accordingly, the nature of the IEC in the magnetic multilayer $\text{Ni}(\text{Cu}(t_{\text{Cu}}))$ Ni\Fe is investigated in more detail in a wedged sample made of Cu(001) Ni(12) Cu (t_{Cu}) Ni(2) Fe(2.5) (see section S8 of the Supporting Information). The epitaxial multilayer grown on a Cu(001) single crystal shows clearly an IEC whose sign oscillates as a function of t_{Cu} (see Figure S10). Based on this observation, the absence of a sign change of the IEC in the multilayers grown on top of MgO single crystals seems to be linked to the presence of the Ir buffer required to stabilize the PMA-Ni layer, which causes a lower quality of the epitaxial growth and possibly of the interfaces in those samples when compared to the full metallic stack. Indeed, the sign

change of the interlayer coupling is the result of complex dynamics of the conduction electrons close to the Fermi surface, influenced by the interfaces of the systems. Our samples are characterized by strain accumulation due to lattice mismatch and strain relaxation across the stack which cannot be modeled by DFT, and this could be the origin of the unexpected absence of an IEC sign change in the experimental observation.

In Figure 3c, the OOP domain state of the top magnet of five different samples is reported as a function of the Cu thickness. Here, each data set originates from a different sample with a fixed t_{Cu} . As expected based on the results shown in Figure 3b, very different magnetic domain configurations are observed in samples with different t_{Cu} . This is consistent with an effective magnetic field acting on the free magnet, whose strength is t_{Cu} -dependent. For t_{Cu} = 8.5 ML, we observe the free layer to have a uniform magnetization pointing down (blue), indicating a strong ferromagnetic coupling with the bottom magnet. For larger t_{Cu} up to 15.3 ML, the coupling is observed to become weaker. Indeed, we observe reversed magnetic domains pointing up (red domains) with different size distributions for different t_{Cu} . Analyzing the magnetic images in Figure 3c, we extract the skyrmion area distributions for the case of t_{Cu} = 11.0, 11.7, 13.5, and 15.3 ML, as reported in Figure 3d (details concerning the extraction of the skyrmion area distributions are reported in section S10 of the Supporting Information). Assuming an ideal circular shape for the magnetic domains, we also extract the corresponding distributions of the effective skyrmion diameters $(2\sqrt{\text{Area}/\pi})$. The median values of the skyrmion area and effective diameter are reported in Figure 3e. The effective diameter is observed to increase with increasing Cu thickness, suggesting the presence of an effective field Beff whose amplitude decreases with increasing t_{Cu} , in the range of thicknesses here considered. It is worth mentioning that the IEC-stabilized magnetic skyrmions are observed not only in the as-grown magnetic multilayers but also after the application of an external magnetic field of 0.5 T (see section S7 of the Supporting Information for more information).

A second sample with $t_{\text{Cu}} = 11.7 \text{ ML}$ and $t_{\text{Fe}} = 2 \text{ ML}$ is prepared to study more in detail the spin texture of the stabilized zero-field ferromagnetic skyrmions. Figure 4a schematically shows the complete materials stack and the experimental OOP magnetic state in the top Fe layer. Figure 4b shows an enlarged image of one of the observed skyrmions, highlighting the domain wall spin texture. The compound SPLEEM image clearly shows a Néel-type skyrmion, with a right-handed rotational sense. In Figure 4c, we report the distribution of the orientation angle (alpha) of the DW magnetization (m) with respect to the normal to the DW (n) at all pixels located on domain wall center-lines in the image in Figure 4a. The plot shows a single peak around alpha = 0° , indicating the presence of DWs with a Néel character, mostly pointing from up-magnetized to down-magnetized domains, which corresponds to a right-handedness (N.R., in Figure 4c). We point out that the handedness of the imaged DWs is in agreement with the DFT calculations above, which indeed predict the stabilization of right-handed DWs in the $Cu(001)\Ni(2)\Fe(2)$ system, as reported in Figure 2. Finally, Figure 4d shows a 3D representation of the magnetization of the same skyrmion in Figure 4b, extracted directly from the experimental data.

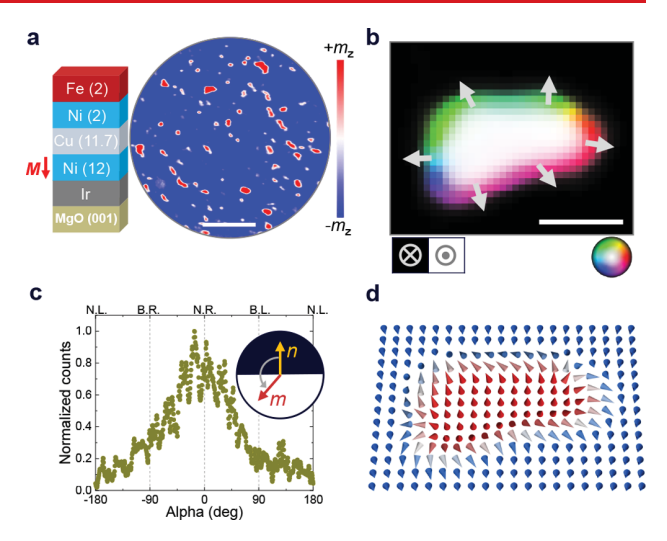


Figure 4. Skyrmion anatomy. (a) OOP magnetic state of a sample whose complete materials stack is shown on the left. The reference layer magnetization is pointing down, as shown by the red arrow. The scale bar is 2 μm . (b) Compound SPLEEM image of one of the observed skyrmions, showing its Néel-type right-handed chirality. The in-plane magnetization orientation is described by the color wheel. The gray arrows indicate the local magnetization direction in the DW. The scale bar is 200 nm. (c) Histogram of the DW magnetization angle distribution for the skyrmions in panel a. The single peak at alpha = 0° shows that the observed magnetic skyrmions are Néel-type with right-handed chirality (N.R. = Néel-Right; N.L. = Néel-Left; B.R. = Bloch-Right; B.L. = Bloch-Left).(d) A three-dimensional representation of the magnetization of the skyrmion in panel b. Each cone represents a 3 \times 3 pixel² area.

The study presented above shows how we can use IEC to stabilize and control the properties of ferromagnetic skyrmions at room temperature without any external magnetic field. However, applications such as magnetic data storage devices also require small (below 100 nm) dimensions of the skyrmions. With this requirement in mind, we explore a new materials system grown on top of a MgO(111) substrate. The interest in (111)-systems is justified by the fact that they offer more flexibility for the type of materials we can use. First, several (111)-textured magnetic systems have been shown to possess an OOP anisotropy, 39,40 which is one of the requirements for a thin-film-based skyrmionic system. Second, the majority of the reported thin-film multilayers with large DMI hosting skyrmions had a (111) texture, with the ferromagnetic layer in direct contact with a heavy metal layer. 4,17,19 Accordingly, we use $[Co\Ni]_n$ multilayers for building the two magnets and Ir for the nonmagnetic spacer. (111)-Oriented $[Co\Ni]_n$ multilayers are known for being very useful, due to their tunable magnetic anisotropy via tailoring of the thickness ratio between the two materials.⁴¹ We grow a reference magnet consisting of $[Ni(3)\Co(1)]_5\Ni(3)$ on top of an Ir(111) buffer layer, resulting in an OOP magnetized system. Analogously to what has been done for the (001) system, after growth, the reference magnet is saturated by a $\mu_0 \mathbf{H} = -0.5 \text{ T}$ magnetic field, which aligns all of the magnetic moments downward. After the deposition of the Ir spacer, we complete the stack by growing the free magnet consisting of a $Co(5)\Ni(3)$ bilayer (see the schematic in Figure 5a).

Three different samples are investigated, with $t_{\rm Ir}$ = 6, 10, and 15 ML, respectively. The magnetic state of the free layer of the three samples is shown in Figure 5b. The sample with the

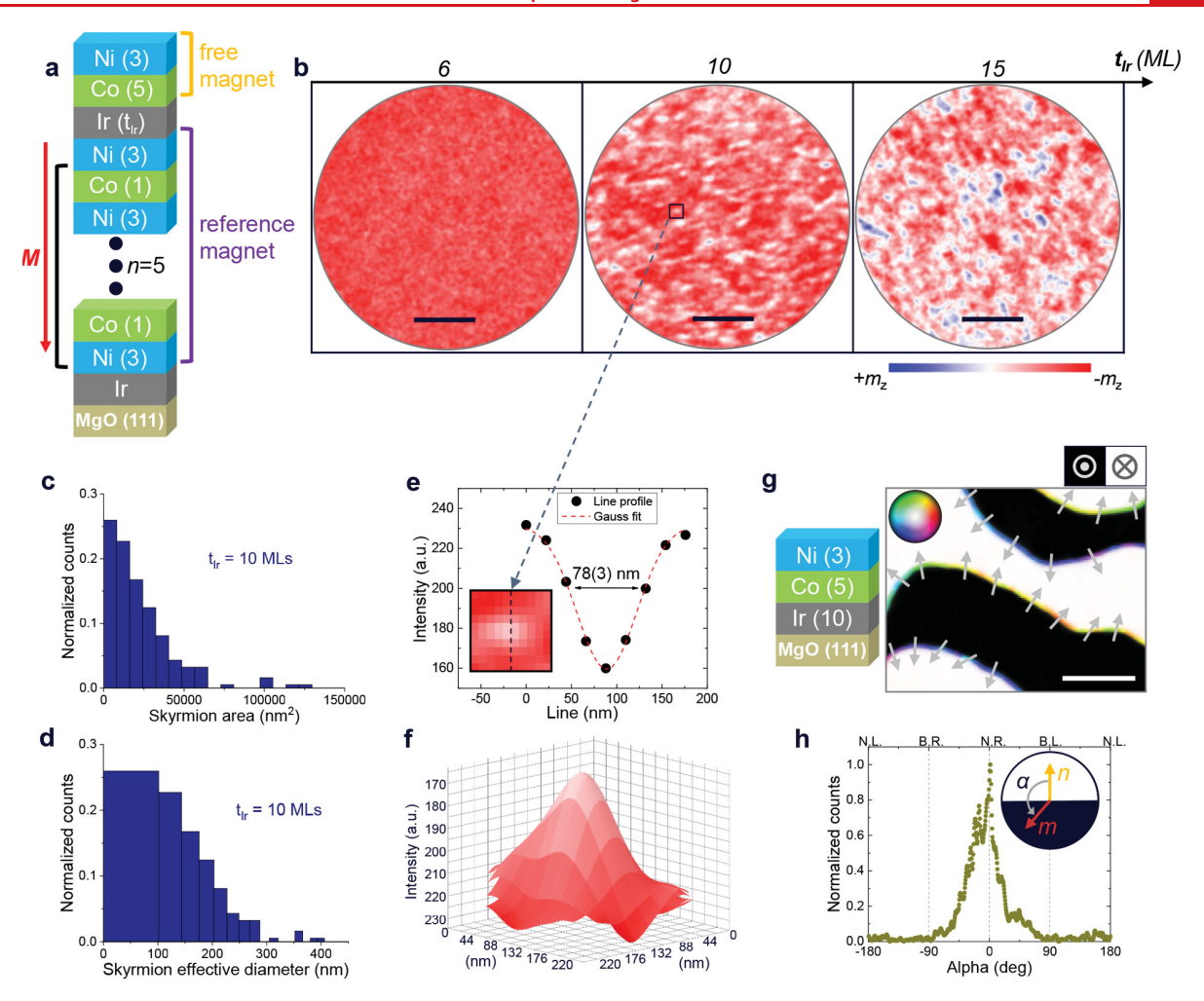


Figure 5. Sub-100 nm zero-field room temperature ferromagnetic skyrmions. (a) Schematic of the (111)-multilayer stacks investigated in this work, made of a magnetic $[Ni(3)\setminus Co(1)]_s\setminus Ni(3)$ reference layer and a $Co(5)\setminus Ni(3)$ free layer. The numbers in parentheses indicate individual layer thicknesses in ML. The reference layer is prepared with its magnetic state pointing down (see small red arrow). (b) Evolution of the OOP magnetic state in the free layer of three samples with different Ir-spacer thicknesses. The scale bar is 1 μ m. (c) Distribution of the magnetic skyrmion area for the sample with $t_{\rm Ir}=10$ ML. (d) Distribution of the effective skyrmion diameter for the same sample in panel c. (e) Line profile of the relative amplitude of the OOP magnetization component across one of the observed skyrmions for $t_{\rm Ir}=10$ ML. The inset shows an enlarged image of the skyrmion. The extracted skyrmion diameter (fwhm) is 78 \pm 3 nm. (f) 2D map of the relative amplitude of the OOP magnetization component of the skyrmion in panel e. (g) Schematic of the multilayer stack used to extract the DW spin texture of the Ir\Co(5)\Ni(3) free layer. In the compound SPLEEM image, the in-plane orientation of the magnetization is represented in color, as described by the color wheel, while black (white) indicates the up (down) orientation of the OOP component. In addition, the gray arrows emphasize the local magnetization direction in the DWs. The scale bar is 1 μ m. (h) Histogram of the DW magnetization angle distribution for the sample in panel g. The single peak at alpha = 0° indicates the presence of right-handed Néel domain walls (N.R. = Néel-Right; N.L. = Néel-Left; B.R. = Bloch-Right; B.L. = Bloch-Left).

thinnest spacer shows a single domain state with magnetization pointing down (red color). This indicates strong ferromagnetic coupling between the reference magnet and the free magnet. The sample with intermediate spacer thickness shows the appearance of small reversed domains (blue-white) pointing up. Finally, for the thickest spacer, larger reversed domains are observed. These observations indicate the presence of an effective field ${\bf B}_{\rm eff}$ which decreases with increasing $t_{\rm Ir}$ for the thicknesses investigated here. The skyrmion area and effective diameter distributions for $t_{\rm Ir}=10$ ML are shown in Figure 5c and d, respectively. Those distributions show that a substantial portion of the skyrmions have a sub-100 nm diameter. A line profile measured from one skyrmion allows us to extract a full width at half-maximum of 78 ± 3 nm via a Gaussian fit (see Figure 5e). Figure 5f plots the relative amplitude of the OOP

component of the magnetization versus the position of the same skyrmion.

In order to extract the handedness of the DWs in the free magnet, we investigate the materials stack MgO(111)\Ir(10)\-Co(5)\Ni(3), as shown in Figure 5g. This system shows wider DWs, which makes it easier for us to resolve their internal spin texture. The observed DW spin texture and the distribution of the DW magnetization orientation angle (alpha) are shown in Figure 5g and h, respectively. As visible in the histogram in Figure 5h, the DW magnetization angle distribution has a narrow single peak around alpha = 0° , indicating that these are Néel DWs with a right-handed rotational sense.

Comparing Figure 4c and Figure 5h, we see that the DW magnetization angle distribution shows a much smaller width of the peak for the Ir(CoNi) system (Gaussian fit width = 35°) than for the Cu(Ni) system (width = 98°; see

section S5 of the Supporting Information). This is evidence of a larger DMI in Ir\[Co\Ni] than in Cu\[Ni\Fe]. Indeed, a stronger DMI results in a larger energy split between Néel and Bloch DW configurations as well as between Néel-right and Néel-left DW configurations. Accordingly, stronger DMI is expected to stabilize non-collinear spin textures which are more robust against thermal fluctuations and pinning effects due to imperfections of the system, resulting in a narrower DW angle distribution, as reported in this work. These findings are in agreement with reports from the literature, where the experimentally extracted DMI for Ir(111)\[Co\Ni]^{42} was found to be 3 times stronger than that for Cu(001)\Ni\Fe.³⁶ The DFT-extracted DMI for $Cu(001)\Ni(2)\Fe(2)$ ($D_{eff} =$ 0.16 meV/atom, see Figure 2b) is in good agreement with the experimental value reported by G. Chen et al. 36 (0.12-0.17 meV/atom), validating the experimentally determined DMI of the two references above and supporting our interpretation. Furthermore, the $Ir\setminus[Co(5)\setminus Ni(3)]$ system shows the possibility to nucleate smaller skyrmions than the Cu [Ni(2)Fe(2)] system, despite the larger dipolar energy of the former due to its larger magnetic thickness.⁴³ Accordingly, the Ir-based stack will be more suitable for applications requiring small and stable isolated skyrmions in the absence of external magnetic fields at room temperature.

In summary, our results show that interlayer exchange coupling (IEC) between a reference and a free magnet can be a powerful tool for stabilizing and tailoring room-temperature isolated ferromagnetic skyrmions without any magnetic field. These multilayers are grown by epitaxy on insulating MgO substrates, which is an important step toward the development of spintronic devices based on zero-field room temperature magnetic skyrmions. Furthermore, the size and the areal density of the nucleated skyrmions can be tuned by tailoring the thickness of the nonmagnetic spacer in between the two magnetic layers. By carefully choosing the materials of the spacer and of the magnets, sub-100 nm ferromagnetic skyrmions can be stabilized at zero-field. This work highlights the possibility to use IEC for the development of skyrmionbased spintronic devices where the tuning of the skyrmion size and areal density across the chip area is desired.

ASSOCIATED CONTENT

Supporting Information

The Supporting Information is available free of charge at https://pubs.acs.org/doi/10.1021/acs.nanolett.0c00137.

More details about sample preparation, DFT calculations, and 3D vector magnetic imaging via spin-polarized low energy electron microscopy (PDF)

AUTHOR INFORMATION

Corresponding Authors

Roberto Lo Conte — Department of Materials Science and Engineering, University of California, Berkeley, California 94720, United States; Department of Physics, University of Hamburg, D-20355 Hamburg, Germany; orcid.org/0000-0002-5050-9978; Email: rloconte.magnetism@gmail.com

Ashis K. Nandy — School of Physical Sciences, National Institute of Science Education and Research, HBNI, 752050 Jatni, India; Email: aknandy@niser.ac.in

Andreas K. Schmid — National Center for Electron Microscopy, Molecular Foundry - Lawrence Berkeley National Laboratory, Berkeley, California 94720, United States; Email: AKSchmid@lbl.gov

Roland Wiesendanger — Department of Physics, University of Hamburg, D-20355 Hamburg, Germany; Email: wiesendanger@physnet.uni-hamburg.de

Authors

Gong Chen – Department of Physics, University of California, Davis, California 95616, United States

Andre L. Fernandes Cauduro — National Center for Electron Microscopy, Molecular Foundry - Lawrence Berkeley National Laboratory, Berkeley, California 94720, United States

Ajanta Maity – School of Physical Sciences, National Institute of Science Education and Research, HBNI, 752050 Jatni, India

Colin Ophus — National Center for Electron Microscopy, Molecular Foundry - Lawrence Berkeley National Laboratory, Berkeley, California 94720, United States

Zhijie Chen — Physics Department, Georgetown University, Washington, DC 20057, United States; orcid.org/0000-0002-3594-5560

Alpha T. N'Diaye — Advanced Light Source, Lawrence Berkeley National Laboratory, Berkeley, California 94720, United States Kai Liu — Department of Physics, University of California, Davis, California 95616, United States; Physics Department, Georgetown University, Washington, DC 20057, United States; orcid.org/0000-0001-9413-6782

Complete contact information is available at: https://pubs.acs.org/10.1021/acs.nanolett.0c00137

Author Contributions

R.L.C. and A.K.N. prepared the manuscript. R.L.C., A.K.N., A.K.S., and R.W. conceived the study. A.K.N. and A.M. performed, analyzed, and interpreted the ab initio DFT calculations. R.L.C., with the support of A.L.F.C., carried out the SPLEEM measurements. R.L.C., C.O., A.L.F.C., and G.C. analyzed and interpreted the SPLEEM results. Z.C., K.L., and A.T.N. carried out magnetic characterizations and helped interpret the SPLEEM results. All authors discussed the results and commented on the manuscript.

Notes

The authors declare no competing financial interest.

ACKNOWLEDGMENTS

R.L.C., A.K.S., and R.W. acknowledge financial support by the European Union via an International Marie Skłodowska-Curie Fellowship (Grant No. 748006 - SKDWONTRACK). A.L.F.C. and A.K.S. acknowledge the support by the Advanced Research Projects Agency-Energy (ARPA-E), U.S. Department of Energy, under Award Number DE-AR0000664. C.O. acknowledges support from the US Department of Energy Early Career Research Program. G.C., Z.C., and K.L. acknowledge support from the US NSF (DMR-1610060 and DMR-1905468) and the UCOP Multicampus Research Programs and Initiatives (MRP-17-454963). The Magnetic Property Measurements System (MPMS3) at Georgetown University used herein was supported by the NSF (DMR-1828420). A.K.N. and A.M. acknowledge financial support from the Department of Atomic Energy, Government of India. A.K.N. thanks Prof. P. M. Oppeneer for the Swedish National Infrastructure for Computing (SNIC) facility. A.K.N. also thanks Dr. Gustav Bihlmayer for the computational support, JURECA at JSC, Forschungszentrum, JULICH. Work at the Molecular Foundry

and at the Advanced Light Source was supported by the Office of Science, Office of Basic Energy Sciences, of the US Department of Energy under Contract No. DE-AC02-05CH11231.

REFERENCES

- (1) Bogdanov, A.; Hubert, A. Thermodynamically Stable Magnetic Vortex States in Magnetic Crystals. *J. Magn. Magn. Mater.* **1994**, *138* (3), 255–269.
- (2) Rößler, U. K.; Bogdanov, A. N.; Pfleiderer, C. Spontaneous Skyrmion Ground States in Magnetic Metals. *Nature* **2006**, 442 (7104), 797–801.
- (3) Mühlbauer, S.; Binz, B.; Jonietz, F.; Pfleiderer, C.; Rosch, A.; Neubauer, A.; Georgii, R.; Böni, P. Skyrmion Lattice in a Chiral Magnet. *Science (Washington, DC, U. S.)* **2009**, 323 (5916), 915–919.
- (4) Romming, N.; Hanneken, C.; Menzel, M.; Bickel, J. E.; Wolter, B.; von Bergmann, K.; Kubetzka, A.; Wiesendanger, R. Writing and Deleting Single Magnetic Skyrmions. *Science (Washington, DC, U. S.)* **2013**, 341, 636–639.
- (5) Fert, A.; Levy, P. M. Role of Anisotropic Exchange Interactions in Determining the Properties of Spin-Glasses. *Phys. Rev. Lett.* **1980**, 44 (23), 1538–1541.
- (6) Fert, A. Magnetic and Transport Properties of Metallic Multilayers. *Mater. Sci. Forum* **1991**, *59*–*60*, 439–480.
- (7) Crépieux, A.; Lacroix, C. Dzyaloshinsky-Moriya Interactions Induced by Symmetry Breaking at a Surface. *J. Magn. Magn. Mater.* **1998**, *182* (3), 341–349.
- (8) Vedmedenko, E. Y.; Udvardi, L.; Weinberger, P.; Wiesendanger, R. Chiral Magnetic Ordering in Two-Dimensional Ferromagnets with Competing Dzyaloshinsky-Moriya Interactions. *Phys. Rev. B: Condens. Matter Mater. Phys.* **2007**, 75 (10), 104431.
- (9) Bode, M.; Heide, M.; Von Bergmann, K.; Ferriani, P.; Heinze, S.; Bihlmayer, G.; Kubetzka, A.; Pietzsch, O.; Blügel, S.; Wiesendanger, R. Chiral Magnetic Order at Surfaces Driven by Inversion Asymmetry. *Nature* **2007**, 447 (7141), 190–193.
- (10) Chen, G.; Schmid, A. K. Imaging and Tailoring the Chirality of Domain Walls in Magnetic Films. *Adv. Mater.* **2015**, 27 (38), 5738–5743.
- (11) Zhang, X.; Cai, W.; Zhang, X.; Wang, Z.; Li, Z.; Zhang, Y.; Cao, K.; Lei, N.; Kang, W.; Zhang, Y.; et al. Skyrmions in Magnetic Tunnel Junctions. ACS Appl. Mater. Interfaces 2018, 10 (19), 16887–16892.
- (12) Huang, Y.; Kang, W.; Zhang, X.; Zhou, Y.; Zhao, W. Magnetic Skyrmion-Based Synaptic Devices. *Nanotechnology* **2017**, *28*, 08LT02.
- (13) Prychynenko, D.; Sitte, M.; Litzius, K.; Krüger, B.; Bourianoff, G.; Kläui, M.; Sinova, J.; Everschor-Sitte, K. Magnetic Skyrmion as a Nonlinear Resistive Element: A Potential Building Block for Reservoir Computing. *Phys. Rev. Appl.* **2018**, *9* (1), 014034.
- (14) Yu, G.; Upadhyaya, P.; Shao, Q.; Wu, H.; Yin, G.; Li, X.; He, C.; Jiang, W.; Han, X.; Amiri, K.; et al. Room-Temperature Skyrmion Shift Device for Memory Application. *Nano Lett.* **2017**, *17*, 261–268.
- (15) Büttner, F.; Moutafis, C.; Schneider, M.; Krüger, B.; Günther, C. M.; Geilhufe, J.; Schmising, C. v. K.; Mohanty, J.; Pfau, B.; Schaffert, S.; et al. Dynamics and Inertia of Skyrmionic Spin Structures. *Nat. Phys.* **2015**, *11* (3), 225–228.
- (16) Jiang, W.; Upadhyaya, P.; Zhang, W.; Yu, G.; Jungfleisch, M. B.; Fradin, F. Y.; Pearson, J. E.; Tserkovnyak, Y.; Wang, K. L.; Heinonen, O.; et al. Blowing Magnetic Skyrmion Bubbles. *Science* **2015**, 349 (6245), 283.
- (17) Moreau-Luchaire, C.; Moutafis, C.; Reyren, N.; Sampaio, J.; Vaz, C. A. F.; Van Horne, N.; Bouzehouane, K.; Garcia, K.; Deranlot, C.; Warnicke, P.; et al. Additive Interfacial Chiral Interaction in Multilayers for Stabilization of Small Individual Skyrmions at Room Temperature. *Nat. Nanotechnol.* **2016**, *11* (5), 444–448.
- (18) Woo, S.; Litzius, K.; Krüger, B.; Im, M.-Y.; Caretta, L.; Richter, K.; Mann, M.; Krone, A.; Reeve, R. M.; Weigand, M.; et al. Observation of Room-Temperature Magnetic Skyrmions and Their Current-Driven Dynamics in Ultrathin Metallic Ferromagnets. *Nat. Mater.* **2016**, *15* (5), 501–506.

- (19) Soumyanarayanan, A.; Raju, M.; Gonzalez Oyarce, A. L.; Tan, A. K. C.; Im, M.-Y.; Petrović, A. P.; Ho, P.; Khoo, K. H.; Tran, M.; Gan, C. K.; et al. Tunable Room-Temperature Magnetic Skyrmions in Ir/Fe/Co/Pt Multilayers. *Nat. Mater.* **2017**, *16* (9), 898–904.
- (20) Woo, S.; Song, K. M.; Zhang, X.; Ezawa, M.; Zhou, Y.; Liu, X.; Weigand, M.; Finizio, S.; Raabe, J.; Park, M.-C.; et al. Deterministic Creation and Deletion of a Single Magnetic Skyrmion Observed by Direct Time-Resolved X-Ray Microscopy. *Nat. Electron.* **2018**, *1* (5), 288–296.
- (21) Caretta, L.; Mann, M.; Büttner, F.; Ueda, K.; Pfau, B.; Günther, C. M.; Hessing, P.; Churikova, A.; Klose, C.; Schneider, M.; et al. Fast Current-Driven Domain Walls and Small Skyrmions in a Compensated Ferrimagnet. *Nat. Nanotechnol.* **2018**, *13* (12), 1154–1160.
- (22) Zhang, X.; Ezawa, M.; Zhou, Y. Magnetic Skyrmion Logic Gates: Conversion, Duplication and Merging of Skyrmions. *Sci. Rep.* **2015**, *5*, 9400.
- (23) Gilbert, D. A.; Maranville, B. B.; Balk, A. L.; Kirby, B. J.; Fischer, P.; Pierce, D. T.; Unguris, J.; Borchers, J. A.; Liu, K. Realization of Ground-State Artificial Skyrmion Lattices at Room Temperature. *Nat. Commun.* **2015**, *6* (1), 8462.
- (24) Boulle, O.; Vogel, J.; Yang, H.; Pizzini, S.; De Souza Chaves, D.; Locatelli, A.; Menteş, T. O.; Sala, A.; Buda-Prejbeanu, L. D.; Klein, O.; et al. Room-Temperature Chiral Magnetic Skyrmions in Ultrathin Magnetic Nanostructures. *Nat. Nanotechnol.* **2016**, *11* (5), 449–454.
- (25) Chen, G.; Mascaraque, A.; N'Diaye, A. T.; Schmid, A. K. Room Temperature Skyrmion Ground State Stabilized through Interlayer Exchange Coupling. *Appl. Phys. Lett.* **2015**, *106* (24), 242404.
- (26) Lemesh, I.; Litzius, K.; Böttcher, M.; Bassirian, P.; Kerber, N.; Heinze, D.; Zázvorka, J.; Büttner, F.; Caretta, L.; Mann, M.; et al. Current-Induced Skyrmion Generation through Morphological Thermal Transitions in Chiral Ferromagnetic Heterostructures. *Adv. Mater.* **2018**, *30*, 1805461.
- (27) Yu, G.; Jenkins, A.; Ma, X.; Razavi, S. A.; He, C.; Yin, G.; Shao, Q.; He, Q. l.; Wu, H.; Li, W.; et al. Room-Temperature Skyrmions in an Antiferromagnet-Based Heterostructure. *Nano Lett.* **2018**, *18* (2), 980–986.
- (28) Brandão, J.; Dugato, D. A.; Seeger, R. L.; Denardin, J. C.; Mori, T. J. A.; Cezar, J. C. Observation of Magnetic Skyrmions in Unpatterned Symmetric Multilayers at Room Temperature and Zero Magnetic Field. *Sci. Rep.* **2019**, *9* (1), 4144.
- (29) Nandy, A. K.; Kiselev, N. S.; Blügel, S. Interlayer Exchange Coupling: A General Scheme Turning Chiral Magnets into Magnetic Multilayers Carrying Atomic-Scale Skyrmions. *Phys. Rev. Lett.* **2016**, 116, 177202.
- (30) Gruenberg, P.; Schreiber, R.; Pang, Y.; Brodsky, M. B.; Sowers, H. Layered Magnetic Structures: Evidence for Antiferromagnetic Coupling of Fe Layers across Cr Interlayers. *Phys. Rev. Lett.* **1986**, *57* (19), 2442–2445.
- (31) Parkin, S. S. P.; Bhadra, R.; Roche, K. P. Oscillatory Magnetic Exchange Coupling through Thin Copper Layers. *Phys. Rev. Lett.* **1991**, *66* (16), 2152–2155.
- (32) Bruno, P.; Chappert, C. Interlayer Exchange Coupling: RKKY Theory and Beyond. In *Magnetism and Structure in Systems of Reduced Dimentions*; Farrow, R. F. C., Ed.; Plenum Press: New York, 1993; pp 389–399.
- (33) Kresse, G.; Hafner, J. Ab Initio Molecular Dynamics for Liquid Metals. Phys. Rev. B: Condens. Matter Mater. Phys. 1993, 47 (1), 558–561.
- (34) Kresse, G.; Furthmüller, J. Efficient Iterative Schemes for Ab Initio Total-Energy Calculations Using a Plane-Wave Basis Set. *Phys. Rev. B: Condens. Matter Mater. Phys.* **1996**, 54 (16), 11169–11186.
- (35) Wimmer, E.; Krakauer, H.; Weinert, M.; Freeman, A. J. Full-Potential Self-Consistent Linearized-Augmented-Plane-Wave Method for Calculating the Electronic Structure of Molecules and Surfaces: O2Molecule. *Phys. Rev. B: Condens. Matter Mater. Phys.* 1981, 24 (2), 864–875.
- (36) Chen, G.; Zhu, J.; Quesada, A.; Li, J.; N'Diaye, A. T.; Huo, Y.; Ma, T. P.; Chen, Y.; Kwon, H. Y.; Won, C.; et al. Novel Chiral

Magnetic Domain Wall Structure in Fe/Ni/Cu (001) Films. Phys. Rev. Lett. 2013, 110 (17), 177204.

- (37) Qiu, Z. Q.; Pearson, J.; Bader, S. D. Oscillatory Interlayer Magnetic Coupling of Wedged Co/Cu/Co Sandwiches Grown on Cu(100) by Molecular Beam Epitaxy. *Phys. Rev. B: Condens. Matter Mater. Phys.* 1992, 46 (13), 8659–8662.
- (38) Bruno, P.; Chappert, C. Oscillatory Coupling between Ferromagnetic Layers Separated by a Nonmagnetic Metal Spacer. *Phys. Rev. Lett.* **1991**, *67* (12), 1602–1605.
- (39) Arora, M.; Hübner, R.; Suess, D.; Heinrich, B.; Girt, E. Origin of Perpendicular Magnetic Anisotropy in Co/Ni Multilayers. *Phys. Rev. B: Condens. Matter Mater. Phys.* **2017**, *96* (2), 024401.
- (40) Gambardella, P.; Rusponi, S.; Veronese, M.; Dhesi, S. S.; Grazioli, C.; Dallmeyer, A.; Cabria, I.; Zeller, R.; Dederichs, P. H.; Kern, K.; et al. Giant Magnetic Anisotropy of Single Cobalt Atoms and Nanoparticles. *Science* **2003**, *300* (5622), 1130–1133.
- (41) Andrieu, S.; Hauet, T.; Gottwald, M.; Rajanikanth, A.; Calmels, L.; Bataille, A. M.; Montaigne, F.; Mangin, S.; Otero, E.; Ohresser, P.; et al. Co/Ni Multilayers for Spintronics: High Spin Polarization and Tunable Magnetic Anisotropy. *Phys. Rev. Mater.* **2018**, *2* (6), 064410.
- (42) Chen, G.; N'Diaye, A. T.; Wu, Y.; Schmid, A. K. Ternary Superlattice Boosting Interface-Stabilized Magnetic Chirality. *Appl. Phys. Lett.* **2015**, *106* (6), 062402.
- (43) Büttner, F.; Lemesh, I.; Beach, G. S. D. Theory of Isolated Magnetic Skyrmions: From Fundamentals to Room Temperature Applications. *Sci. Rep.* **2018**, *8* (1), 4464.